

Proposal Report

Characterisation of NGC 4826

Albert Álvaro Díaz
and
Tomás Riera Gómez

Master in Theoretical Physics
Astrophysics Specialty

Academic year 2023-2024

Abstract

In this report we show the results obtained on the field trip to the Calar Alto observatory in Almería for the NGC 4826 project. We detail the technical aspects of our work and data reduction, both in photometry and spectroscopy, and try to look into certain physical properties like the magnitude, the luminosity profile or the existence of certain elements in the galactic disk and bulb.

Contents

1	Scientific goals	1
1.1	Photometry	1
1.2	Spectroscopy	2
2	Data reduction	3
2.1	Photometry	3
2.2	Spectroscopy	7
3	Results and Analysis	14
3.1	Photometry	14
3.1.1	Integrate Apparent Magnitude	14
3.1.2	Flux Profile and Sersic Profile	14
3.1.3	Color Image	16
3.2	Spectroscopy	16
3.2.1	Full galactic spectrum	16
3.2.2	Bulb spectrum	17
3.2.3	Galactic Disk	17
4	Bibliography	24

1 Scientific goals

Our general goal is to study and characterize in different ways the galaxy NGC 4826, also named Messier 64. With this aim we performed photometric and spectroscopic measurements of the object, processed the data, and tried to extract physical information from it. In this section we detail the main goals of this project for the different measurements and the specifications that we needed at the observatory to perform successfully the mentioned images.

First of all, we want to emphasize the fact that some initial goals from the initial proposal have not been able to be carried out for different factors which we will detail during this report. Some of this factors will be the absence of reduction image (flat) or the lack of accuracy from some of the measurements.

1.1 Photometry

We are going into detail of photometry specifications of the exposures performed.

Initially, we proposed one frame for each band, however, in the observatory we could take one frame more for each band with larger exposure time. The exposure time (1) proposed (see Table 1) was supposed to ensure absence of saturated pixels at the FOV, in this way, we ensured the existence of calibrations stars. The second exposure time (2) was performed to improve the signal to noise ratio in the galaxy bulge, without worrying about the calibrations stars. With this method we could ensure the existence of calibration stars and a good resolutions for the galaxy bulge. The specifications are listed in Table 1.

SDSS Filter	Exposure time 1 (s)	Exposure time 2 (s)
I	15	25
R	35	45
G	95	120

Table 1: Photometric specifications

Eventually, and as we will mention after, we were able to find enough calibration stars, which are not saturated, in the images performed with the second exposure time, therefore, we will only deal with these images.

In order to characterise our astronomical object, we have obtained a few physical magnitudes which are listed as follows. Hereafter we only describe in general terms the goals performed, for more details see the following sections.

1. Understand the reduction and calibration development. The reduction and calibration process is detailed during this report, starting with the raw image obtained from the observatory and eventually reaching to a physical image in physical units.
2. Integrated Apparent Magnitude: An important characteristic of astronomical objects is the apparent magnitude, in this case, the object corresponds with extended source, therefore, we have to compute the integrated flux over the galaxy and hence calculate the magnitude for each band.
3. Flux Profile and Sersic Profile fitting. Another important characteristic which describes the different type of galaxies is the Sersic Profile fitting. The profile mentioned describe the evolution of flux as a function of distance from the center of the galaxy. With a fit

of this profile over the data of our astronomical object we obtain the Sersic parameters which describe the NGC 4826 galaxy.

4. Color Image. As it showed above the filters performed are located on the optical range, hence, we can associate each band for the RGB bands in order to obtain a color image of our astronomical object.

1.2 Spectroscopy

The spectroscopic measurements of the galaxy were scarce due to lack of time and bad weather. Our science image is a single exposure of 1500 s using the G-200 grism of CAFOS, as shown in Table 2. Given the fact that this is a short exposure time for an accurate spectroscopic measurement, we would like to emphasize that the resolution attained is not the highest, however it did allow for a proper obtention and calibration of the spectrum and the observation of different elements' lines. Hence the spectroscopic objectives can be summed up as:

1. Understand the spectroscopic reduction and calibration of data.
2. Learn to find different lines in the galactic spectrum and the dependence on position on the galaxy
3. Look into how the different parts of the galaxy emmit with different strengths, and at different wavelengths

For the calibration, the star HD 93521 was used, since it was measured in the same night with the same filter. A more detailed explanation of the whole procedure is shown in section 2.2.

Grism	Exposure time (s)
G-200	1500

Table 2: Spectroscopic specifications

2 Data reduction

2.1 Photometry

In this section we are going into the details about the process of raw science photometry reduction and calibration in physical magnitudes, in order to assess different characteristics of our object.

First of all, an example of an NGC 4826 raw science image is introduced in Fig (1), as taken from the observatory and without any processing.

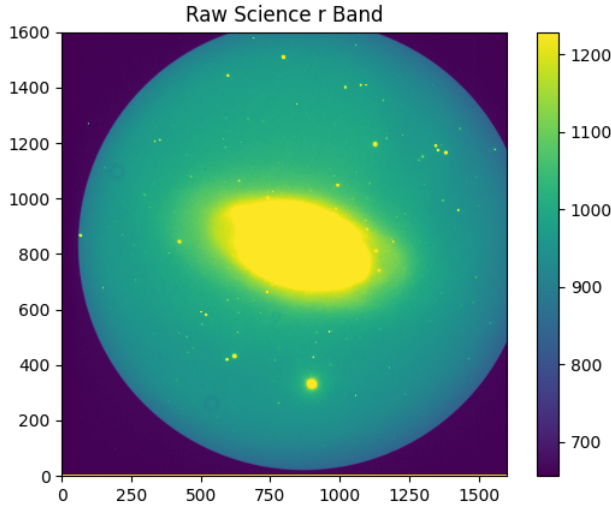


Figure 1: Raw Science Image in r Band

For a general image reduction, the first step is to subtract the bias and dark current over the exposure time and divide this by the flat multiplied by the exposure time. In general terms, the bias measures the offset (in counts) introduced to avoid negative values, the dark measures the thermal current produced due to the temperature of the detector, and the flat measures the sensitivity and irregularities of the detector (e.g dust particle on the filter or detector). In our case, the CCD (detector) is cooled around -60°C , therefore, we can set the dark current to 0. The normal way to proceed at the observatory is take a few images of bias, which correspond with set 0 the exposure time and with the dome closed. In the same way, for the flats, a few images for each band are taken.

In order to subtract this quantities over the raw image, we have to apply the median over the bias images, thereby we obtain an image called *master bias*. In this median we ignore the NaN (saturated) values. This process, for the *master flat*, is slightly different. For each flat from each band, firstly we have to subtract the master bias and consecutively normalise the image over the mean of the image itself. The images mentioned are shown in Fig. (2). Once the master bias and master flat for each band are obtained, the next step is subtract these quantities from the raw image.

As we know, each science image is taken with different exposure times, depending on the sensitivity of the detector for each band. When we take an image at the observatory, the retrieved image is in units of *counts*, these quantities depend on the exposure time, hence, we have to normalise over the time mentioned, in order to obtain a retrieval in units of *counts/s*. The treatment mentioned is resumed with the following equation:

$$I_{reduced} = \frac{I_{raw} - Bias - Dark \cdot t_{science}}{Flat \cdot t_{science}} \quad (1)$$

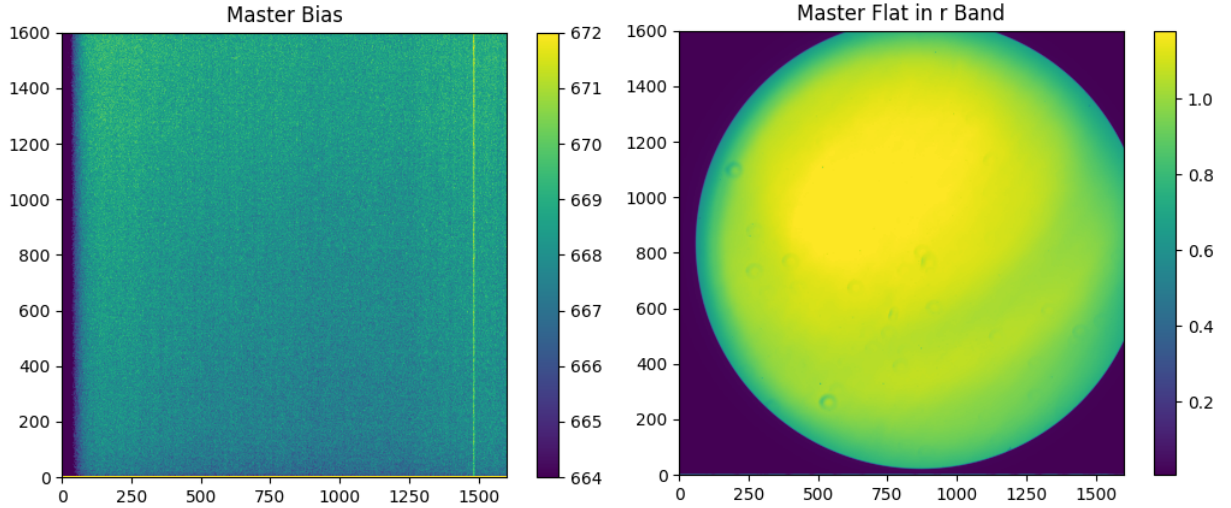


Figure 2: In the left panel is shown the *master_bias* and in the right panel the *master_flat* in r band as example

Where I is the science image, $Bias$ and $Flat$ are the master bias and master flat mentioned above respectively, $Dark$ is the dark current (remember we have set it as 0) and $t_{science}$ is the exposure time for the science image. Following the description above we obtain the reduced science image, which is shown in Fig. (3).

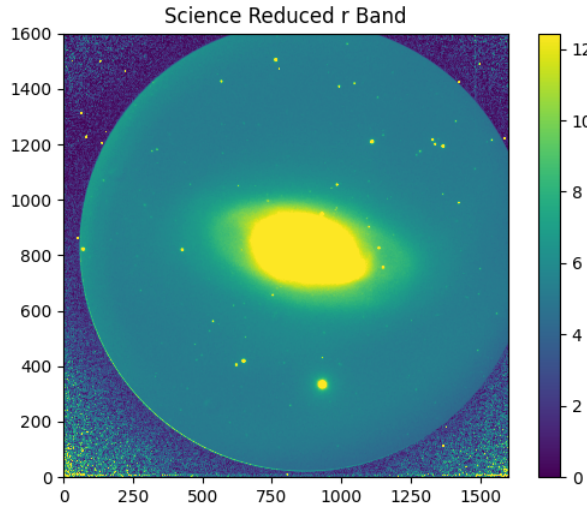


Figure 3: Science Image reduced of Bias, Dark and Flat.

Subsequently, we have to subtract the characteristic brightness of sky. To do so, we select an area of our image of Fig. (3) and compute the mode of the pixels confined. It is important to bear in mind two statements on this step: On one hand, take an area large enough to compute statistical methods correctly. On the other hand, try to choose an area without counts sources (as stars, galactic dust, galaxies...). In our case, we chose a lower left area of 200×200 pixels. With this process is obtained and image shown in Fig.(4).

Up to this point, we have reduced the image from the different counts sources, with the aim to obtain a image with, supposedly, only the counts from our astronomical object. Hence, we can begin with the calibration process. Before to showing the retrieval image, we detail, in general terms, the development of the calibration.

Typically, we need calibration stars. We can find this in the same field of view (FOV) of

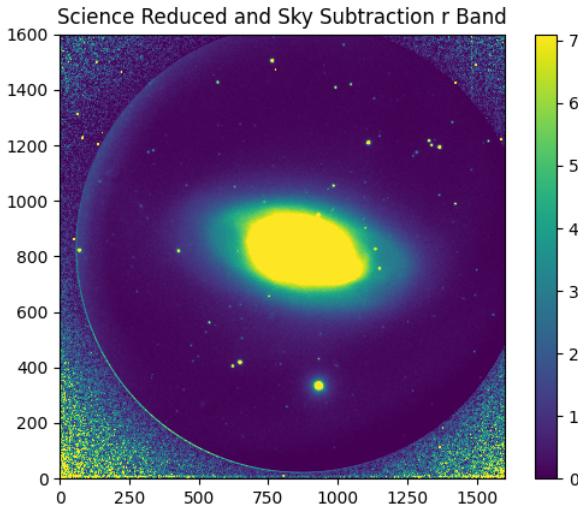


Figure 4: Image after Sky subtraction in r Band

the science image or, previously, we have had take a few shots of the stars mentioned. In our case, we could find calibrations stars in the FOV.

The calibration stars are astronomical objects which the magnitude (or flux) in the interested bands are known by differente astronomical catalog. In our case, we could find 4 of this stars in the Lamost LRS catalog [3] from ESA Sky [4]. The selected calibration stars are shown in Fig. (5).

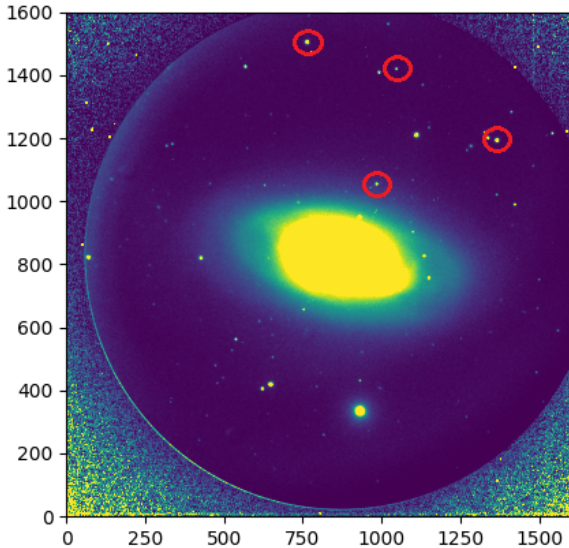


Figure 5: FOV image with the calibration stars marked

As it mentioned, the magnitude of calibrations stars are known from the astronomical catalog. As we know, the unit of *magnitude* does not have physical meaning, and hence, it is convenient compute the flux in units of $\text{erg}/\text{s}/\text{cm}^2$ via the following expression:

$$F(\lambda) = 10^{-0.4 \cdot \text{Mag}(\lambda)} \cdot F_0(\lambda) \quad (2)$$

Where Mag and F is the calibration star magnitude and flux respectively, and F_0 is the reference flux of the reference null magnitude of the system used, in this case, Vega System. We express the flux as $F(\lambda)$, and magnitude as well, to emphasise the fact that, the expression above is for each band. The quantities of references fluxes (F_0) come from the zero point of the

system and the full width at half maximum (FWHM) of filter used, this values are tabulated, one may find it in [2].

Once the calibration stars are selected, we have to find it over the science image, as shown before in Fig. (5), and integrate the pixels which correspond with the calibration star. We have to repeat this process for all the calibration star. Eventually, we have, for each star and for each band, the number of *counts/s* and the flux (obtained from Eq. (2)). We can compute the relation of this quantities via:

$$C_{cal} = \frac{F_{physical}[erg s^{-1} cm^{-2} A^{-1}]}{F_{counts}[counts s^{-1}]} \quad (3)$$

In this case, for each band we have four calibration stars, and hence, four calibration constants (Eq. (3)). We can compute the median of these array of constant, thereby, we obtain one C_{cal} for each band.

Afterwards, it compute $C_{cal} \times I_{reduced}$ for each band, where $I_{reduced}$ correspond to the image reduced completely as shown in Fig. (4), in this way, we obtain our astronomical object image calibrated in flux units. This image is shown in Fig. (6).

One could reverse Eq. (2) in order to obtain an image calibrated in apparent magnitude. This image can be seen in Fig. (6).

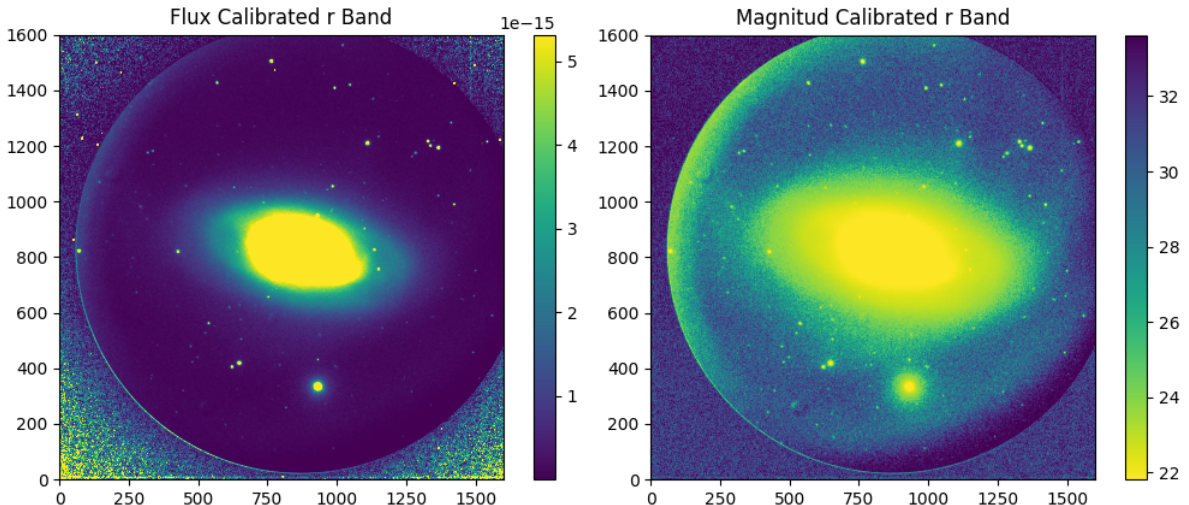


Figure 6: Left panel flux calibrated science image and right panel apparent magnitude calibrated science image

After some effort it is acquired our astronomical object (NGC 4826) calibrated in flux and apparent magnitude.

2.2 Spectroscopy

For the data reduction it is important to note that all calibration images had the same detector area (i.e. pixel dimensions) as the science image, so no trimming had to be done. This section is USERDEF2. Furthermore, we remember that the dark current is negligible. The data reduction begins with 9 bias files, 5 flat files, one arc image and one science image, as we took a single, 1500 s exposure. Given the short exposure time, we expect the spectrum to be poorly resolved. The only reduction is to be done on this science file. The steps of the reduction were as follows:

- The master bias is obtained by calculating the median of all the bias files. More specifically, the command `numpy.nanmedian` was used to calculate the median of all the bias files excluding the nan values. This gives the master bias image shown in the left panel of figure 7.

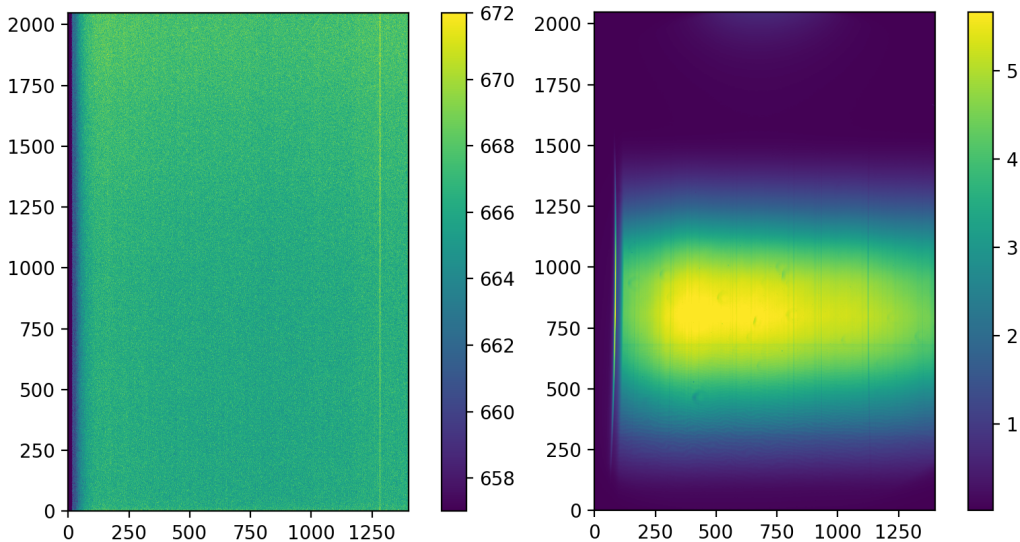


Figure 7: Left panel shows the master bias image. Right panel shows the master flat image.

- For the flats, as was done in photometry, we subtracted the bias from all flat files and then divided each one by their own median (more specifically, their `numpy.nanmedian`) to normalise them with respect to themselves. Then, the (nan)median of all these was calculated to obtain the master flat show in the right panel of figure 7.
- The science image was reduced by subtracting the master bias from the science image and then dividing this by the product of the master flat and the science exposure time $t_{science}$, i.e.:

$$science_{reduced} = \frac{science_{raw} - masterbias}{masterflat \cdot t_{science}} \quad (4)$$

In figure 8 we show the reduction process. The top left panel shows the raw science image and the top right panel the reduced one.

This whole process is made automatic inside a function for any introduced image, as we will need to do the reduction for the science image and the calibration star image. From here on, we will only take a section of the image: vertically we take pixels between 100 and 1450 as shown in the bottom panel of figure 8 in order to only extract reliable information.

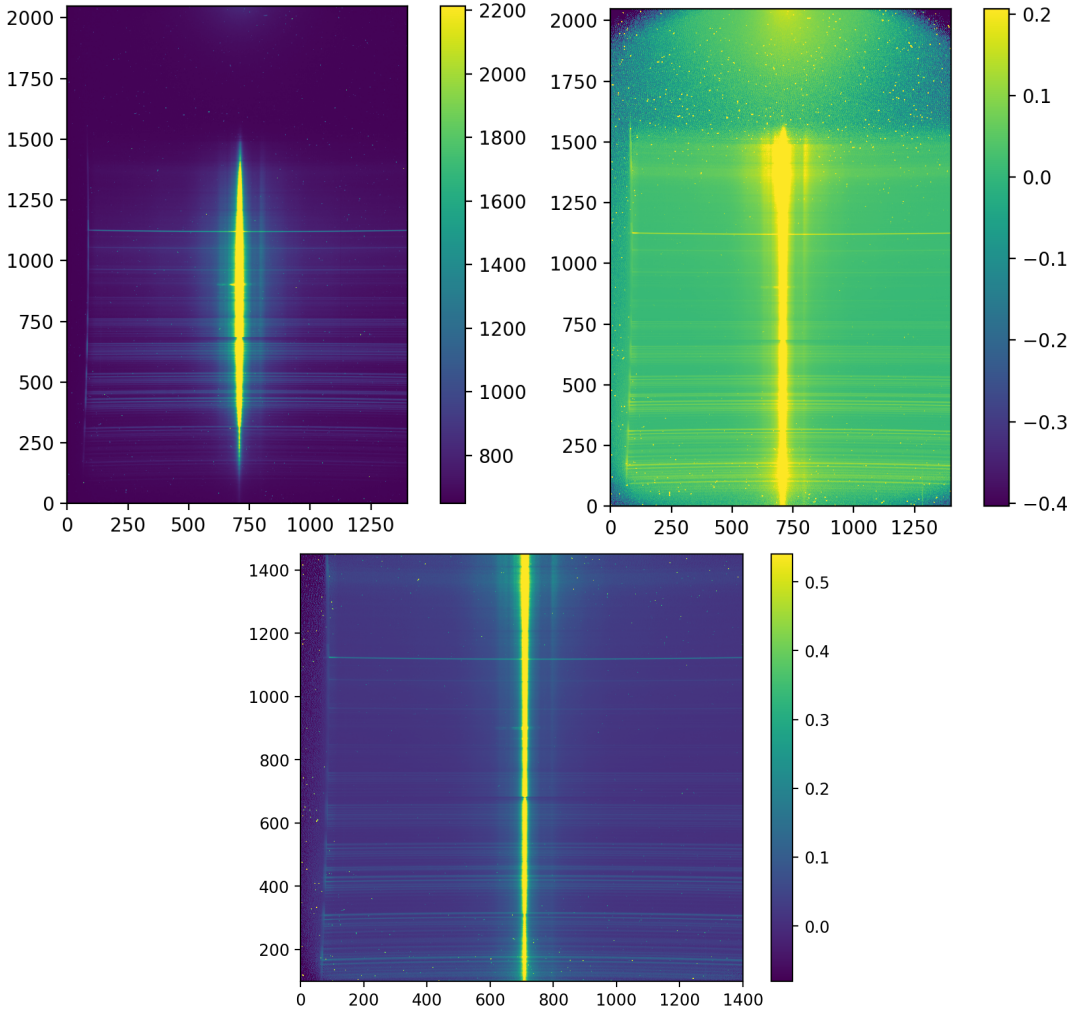


Figure 8: Top left panel shows the raw science image. Top right panel shows the reduced science image, obtained using the steps from equation 4. The bottom panel shows the section of (reduced) science image used. Note we removed the top and bottom pixels, as they do not contain reliable information.

We now need to extract the spectrum in counts/s. As we will see in the results section, we will investigate the spectrum of different parts of the galaxy and the whole (integrated) spectrum. In doing so, we need to take a vertical strip (which can even be of a single pixel width) of the image and sum horizontally to find the 1-d spectrum. We then wavelength-calibrate this using the arc image and the CAFOS lamps' peak spectrum wavelengths. If we look at the bottom panel of figure 8, we see that the spectrum slightly bends at the left and right ends of the slit in opposite (up and down) directions. This is due to the instrument and is something we aimed to correct for the data analysis, since depending on where on the slit we are looking at the spectrum the wavelength calibration becomes different. To do so, we first consider the arc image shown in the top left panel of figure 9. We note that the lamp lines also bend in the same way due to the instrument. Hence, for the wavelength calibration of any strip, we take the same strip of the arc image: hence the degree of bending at this position will be the same. The calibration is done using this strip of arc image and the bending is hence corrected. This dynamical wavelength calibration is automated and allows for us to take any strip and automatically calibrate the corresponding spectrum, mapping the pixels to the correct wavelengths independently of instrumental effects.

The pixel-wavelength mapping is done as follows. Firstly we extract the strip and sum

horizontally over it, obtaining the spectrum as a function of pixel. In order to do the mapping, we need the pixel position and wavelength of each peak of the spectrum. To locate the peaks pixel positions we use `scipy.signal.find_peaks` and select several to compare the pixel positions and the wavelength positions from the CAFOS lamps. An example of such calibration is shown in the bottom panel of figure 9: we show the (normalised) spectrum of an arc strip (summed over the horizontal dimension), with the located peaks marked as red lines and the selected ones as black dashed lines. In all cases the selected peaks were those corresponding to:

$$[5085.82, 5460.74, 5875.618, 6438.47, 7800.268, 7947.603, 8521.162, 10024.35, 10139.8] \text{ \AA}$$

Having the peak pixel positions and their corresponding wavelength positions, we perform for each wavelength calibration a fit of a 5th order polynomial to these points, obtaining a function which accepts as input the pixel positions and returns the corresponding wavelengths. As mentioned, this is done separately for any strip given the instrument's bending of the spectrum.

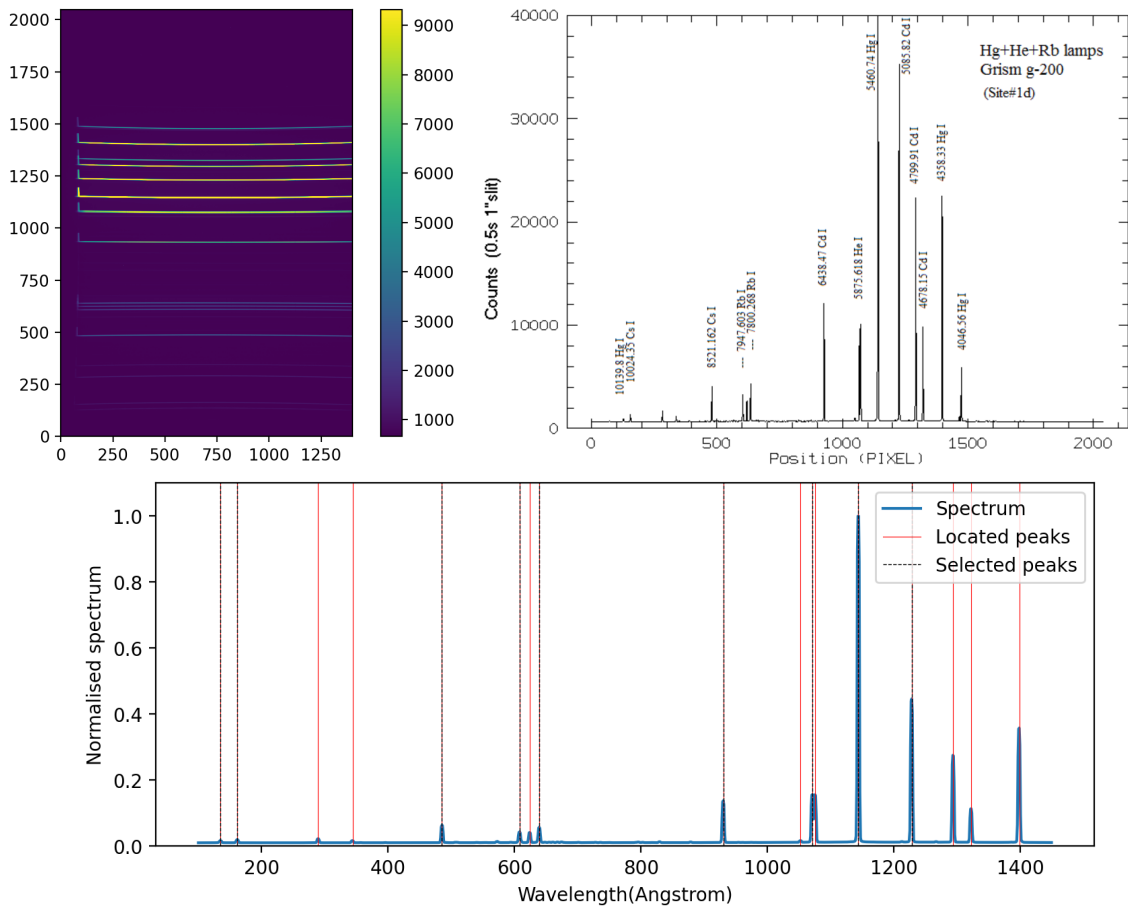


Figure 9: Arc image: CAFOS lamp lines (top left panel), CAFOS g200 Hg+He+Rb lamp reference spectrum (top right panel, taken from <https://w3.caha.es/CAHA/Instruments/CAFOS/comp.html>) and calibration example (bottom panel).

In every spectra taken, we need to subtract the sky spectra before performing the analysis. To do so, we select a 'sky strip', extract its spectrum (summing over the horizontal direction), wavelength-calibrate it (with the corresponding arc strip, as mentioned) and perform the operation:

$$sky_{calib} = \frac{data\ pixel\ width}{sky\ pixel\ width} \cdot sky_{raw}$$

therefore accounting for the difference in pixel coverage of the sky and the data. We note that for this operation we need the data spectrum and the sky spectrum to be defined at the same wavelengths. The correction due to the bending of the light makes the wavelength arrays on which the sky and data are defined to be slightly different. This problem is overcome by interpolating the sky spectrum onto the data wavelength's grid, therefore making the data and sky arrays operable with each other and being able to perform the mentioned operation. An example of strip choosing is shown in figure 10. Having subtracted the sky, there is only one last calibration step required: flux calibrating the spectrum.

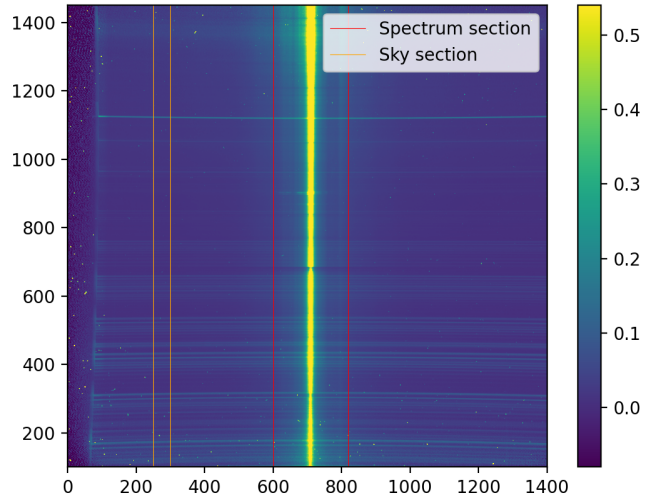


Figure 10: Example of data and sky strip selection

Flux calibration consists on taking a calibration star's spectrum measured in the same night with the same setup and comparing the measured spectrum with a theoretical model for it's atmosphere (i.e. its real spectrum). These models are available publicly and are called Castelli-Kurutz models (see <https://www.stsci.edu/hst/instrumentation/reference-data-for-calibration-and-tools/astronomical-catalogs/castelli-and-kurucz-atlas> for an atlas of the models), and exist as a function of effective temperature, surface gravity and metal abundance [M/H]. We choose the appropriate model, extract its spectrum and compare (divide) it with the measured star's spectrum¹. In doing so we obtain the response curve, which is a measure of the sensitivity of the instrument as a function of wavelength. This allows us to, at last, obtain the true spectrum in flux units instead of counts per second as we have it now. For the calibration we took the star HD 93521, whose spectrum was taken on the same night using the same grism. This is an O9.5 III star which has an effective temperature of $T_{eff} \approx 33000$ K, surface gravity $\log(g) \approx 4$ and $\log([M/H]) \approx -2.5$ (see [1]). We hence take the corresponding Castelli-Kurutz model spectrum and translate it to how we would see it on earth. The atlas suggests us to perform the following operation on the spectrum:

$$F_{model} = F_{CK} \cdot \left(\frac{R}{D} \right)^2 \cdot 3.336 \cdot 10^{-19} \cdot \frac{\lambda^2}{4\pi}$$

where F_{CK} is the Castelli-Kurutz spectrum as extracted directly from the atlas file, R the radius of the star, D the distance to the star, and λ the wavelength. The factor $\left(\frac{R}{D} \right)^2$ accounts for the loss of flux on the light's path to earth and the factor $3.336 \cdot 10^{-19} \cdot \frac{\lambda^2}{4\pi}$ accounts for the conversion to our desired units, $\text{ergs cm}^{-2} \text{s}^{-1} \text{A}^{-1}$, from the units in the file (see

¹Previously having extracted the sky spectrum from the calibration star's spectrum

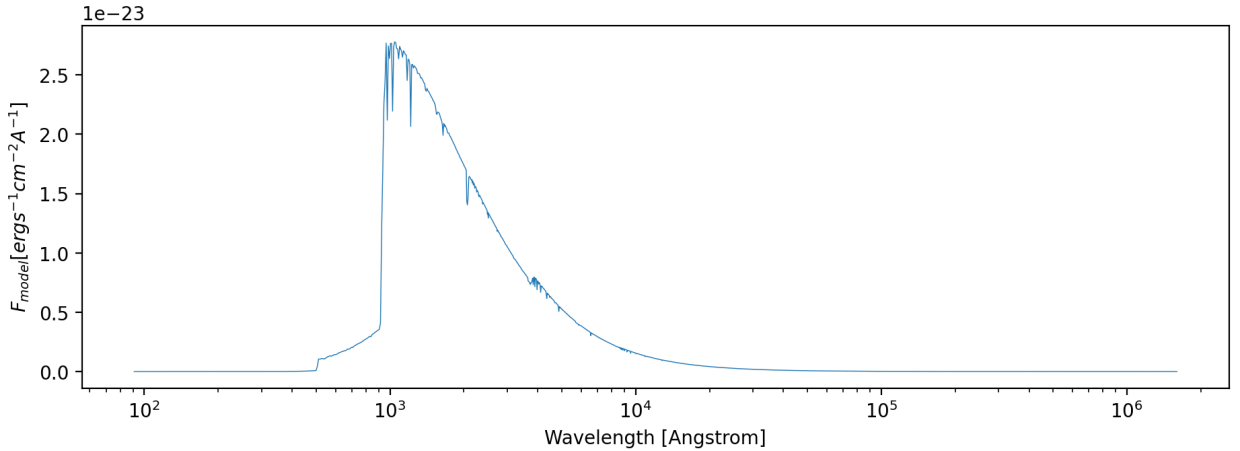


Figure 11: Castelli-Kurutz model used for flux calibration, with effective temperature of $T_{eff} \approx 33000$ K, surface gravity $\log(g) \approx 4$ and $\log([\text{M}/\text{H}]) \approx -2.5$ (see [1]).

<https://www.stsci.edu/hst/instrumentation/reference-data-for-calibration-and-tools/astronomical-catalogs/castelli-and-kurucz-atlas> for more details). In our case $R \approx 7R_\odot$ and $D \approx 1.52\text{kpc}$. The resulting spectrum is shown in figure 11.

The largest complication in this process was to evaluate the model at the wavelength points of our data instead of the ones provided in the file, while maintaining the flux conserved. To do so, we obtain a "cumulative flux", i.e. calculate the cumulative sum of the model flux, interpolate this cumulative flux onto the wavelength grid set by our data, and lastly undo this cumulative sum (by using `numpy.diff()`). We hence have obtained the Castelli-Kurutz spectrum evaluated at the wavelength points of our data and kept flux conservation untouched. Having all this, we can proceed to divide the reduced calibration star's flux by the Castelli-Kurutz flux at earth, obtaining the response curve.

In figure 12 we show the calibration star reduced image, with data and sky strips in the top panel, where the red lines and orange lines indicate the edges of the strip; the calibration star and sky spectrum scaled to the star's pixel range in the middle panel, and the sky-subtracted calibration star spectrum in the bottom panel. We note that the sky spectrum is negligible. Although the reason for this is not known, an error in the data processing has been discarded as a possibility since, as we will see in the results section, for images with a more clear sky spectrum it is correctly calculated. The lack of a sky spectrum is likely due to bad weather conditions, like slight cloudiness or high humidity affecting the measurement. The bottom panel shows the spectrum in counts per second which we will use to flux calibrate our image. Having obtained all this, we calculate, using the procedure mentioned above, the conserved Castelli-Kurutz model flux interpolated onto the calibration star's wavelength grid. This is shown in the top panel of figure 13. Furthermore, having done the interpolation we proceed to divide this function by the star's flux in order to obtain the response curve of the detector, in units of $\text{erg cm}^{-2} \text{A}^{-1} \text{counts}^{-1}$ with which we will calibrate all our spectra. This curve is shown in the bottom panel of figure 13. We note that there is a certain degree of noise, especially at longer wavelengths. We can attribute this to the fact that firstly the Castelli-Kurutz model might be a good fit but still not perfect to the star we're using to calibrate, with the added complication that the measurements were not taken in long exposures: we hence do not have the best resolution so we expect our measurements to be good but their accuracy could be increased with an enhanced resolution and integration times. By multiplying this response curve by any of our measurements, we will, at the same time, subtract from the spectrum the deviations introduced by the sensitivity of the detector to different wavelengths, while also changing it from units of counts per second to real flux units, i.e. $\text{ergs cm}^{-2} \text{s}^{-1} \text{A}^{-1}$.

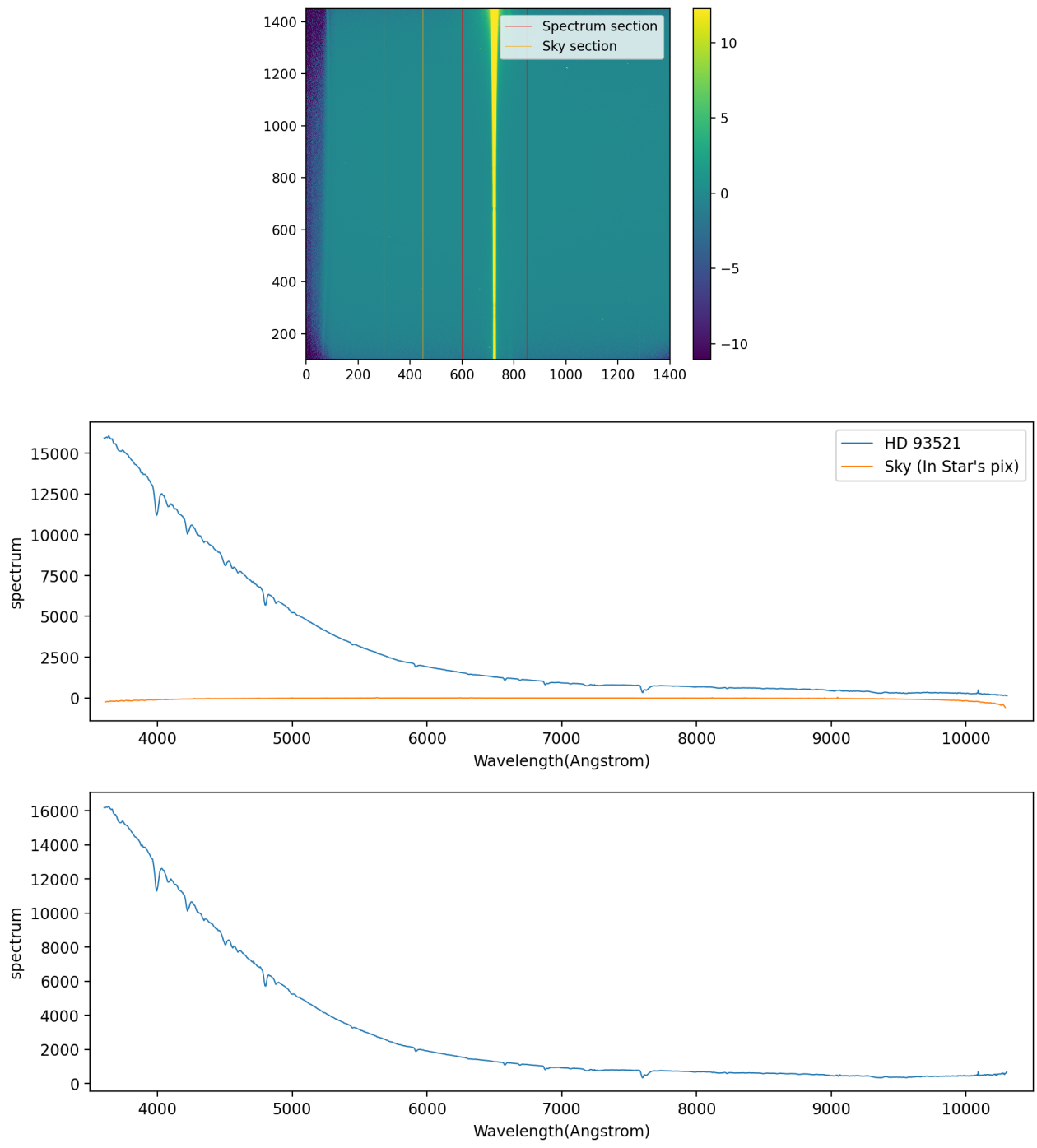


Figure 12: Calibration star reduced image with data and sky strips (top panel, red lines and orange lines indicate the edges of the strip), calibration star and sky spectrum scaled to the star's pixel range (middle panel), and sky-subtracted calibration star spectrum (bottom panel).

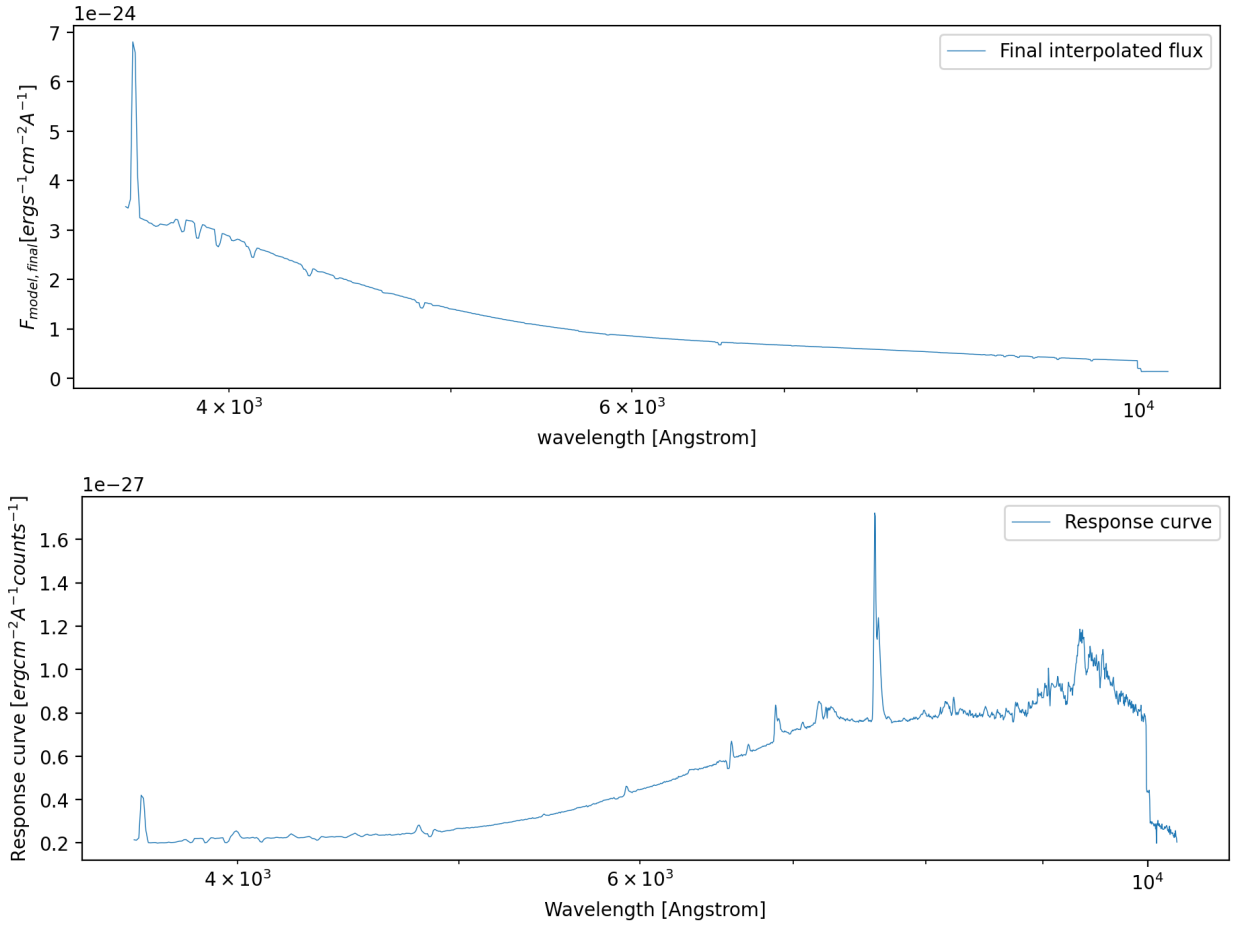


Figure 13: Top panel shows the conserved interpolated Castelli-Kurutz flux onto the calibration star's wavelength grid, i.e. the result of performing the cumulative sum of the flux from figure 11 (the Castelli-Kurutz model), them interpolating this onto the wavelength grid set by the calibration star's spectrum, and then undoing the cumulative sum using `np.diff`. The bottom panel shows the response curve of the detector.

3 Results and Analysis

3.1 Photometry

In this section we details the results obtained and a brief analysis of the results itself. As long as our reduction and analysis we found a few issues. one of them is the absence of flat in filter i. In the following, some results for the i band are shown. This results are displayed only for completeness, for the reader information, i band results could be far from reality.

3.1.1 Integrate Apparent Magnitude

In order to estimate the integrated magnitude of our astronomical object we have to integrate the flux over all galaxy pixels. It is defined the boundary of the galaxy as the isophote of magnitude 25. To estimate the boundary mentioned we have represented the magnitude in function of center distance over two approximated axis of the ellipse. This diagram is shown in the left panel of Fig. (14) and the magnitude in the right panel.

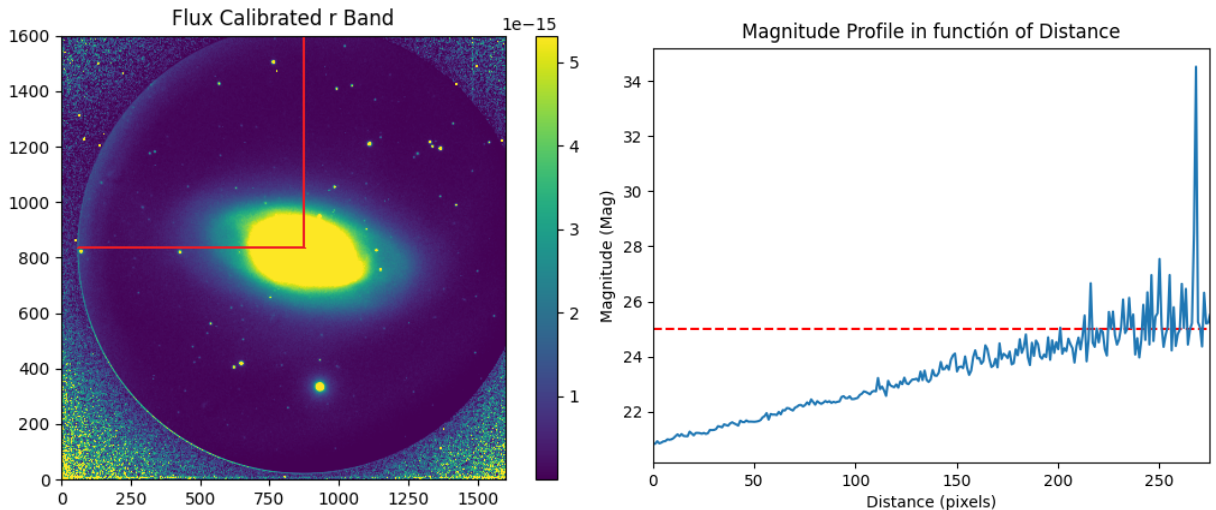


Figure 14: Left panel shows the diagram of the approximates ellipses axis and right panel shows the magnitude profile for vertical axis.

The right panel correspond with the vertical axis. As we can see, the isophote of magnitude 25 is reached at approximately 230 pixels. For the horizontal line we found a distance of 490 pixels. We the measurement mentioned, we can approximate the ellipse to integrate the galaxy. It is important to bear in mind the measurements mentioned depend on the band used. The integrated magnitude obtained are listed in the following table.

Filter	Integrated Magnitude
i	7.82
r	8.14
g	8.69

An example of mask aperture is shown in Fig. (15).

3.1.2 Flux Profile and Sersic Profile

Others physical magnitudes which are estimable are the fit of the Sersic Profile. Once we have our astronomical object calibrated in physical units, we can obtain the Flux profile which

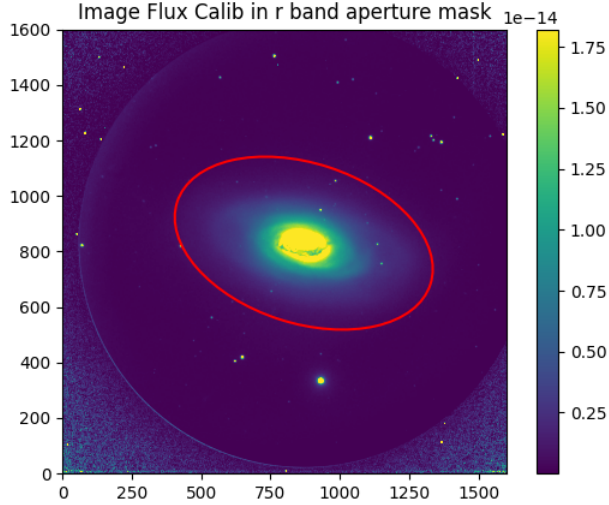


Figure 15: FOV image with integration aperture mask in r band

consists in study the dependence of the Flux over the distance to galaxy centre. Firstly, lets introduce the Sersic profile as following:

$$I(r) = I_e \cdot \exp \left[-b_n \left(\left(\frac{r}{R_e} \right)^{1/n} - 1 \right) \right] \quad (5)$$

Where I_e is the flux at radius R_e , n and b_n are the Sersic parameters.

As it mentioned before, we fit our data over the equation above. For the different bands the results of the fit are listed in the following table:

Filter	I_e	b_n	n	R_e (ly)
i	$1.983 \cdot 10^{-14}$	$1.204 \cdot 10^{-02}$	$8.396 \cdot 10^{-01}$	$1.854 \cdot 10^{+02}$
r	$2.196 \cdot 10^{-14}$	$1.830 \cdot 10^{-01}$	$7.444 \cdot 10^{-01}$	$2.073 \cdot 10^{+03}$
g	$1.757 \cdot 10^{-14}$	$7.203 \cdot 10^{-01}$	$7.642 \cdot 10^{-01}$	$5.819 \cdot 10^{+03}$

The reader can find an example of Flux profile and a Sersic fit in Fig. (16)

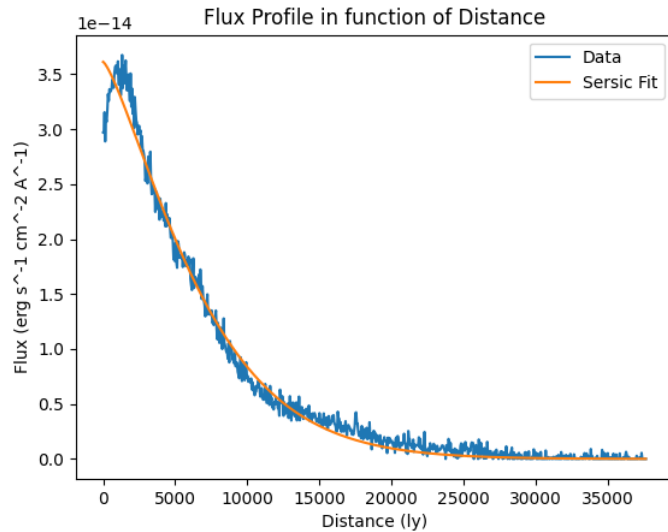


Figure 16: Flux profile as a function of distance from galaxy center with Sersic Profile fitting

3.1.3 Color Image

As it mentioned in the previous chapters, we have three optic bands (i, r, g of SDSS) of our astronomical object. We can compute a color image stacking the bands mentioned and associating each band to each light color band RGB. Initially we did it, but we found and misalignment of the different bands. The reader can see the image in the left panel of Fig. (17).

In order to correct the effect mentioned, we did a ‘homemade’ algorithm based on select the same two stars for each band. The scrip calculates the relative vector between the stars selected, consecutively, it lefts one band as reference and computes the relative angle between the reference band and the rest of them. Finally, the scrip rotates and translates the bands to the same positions as the reference. The result is shown in the right panel of Fig. (17).

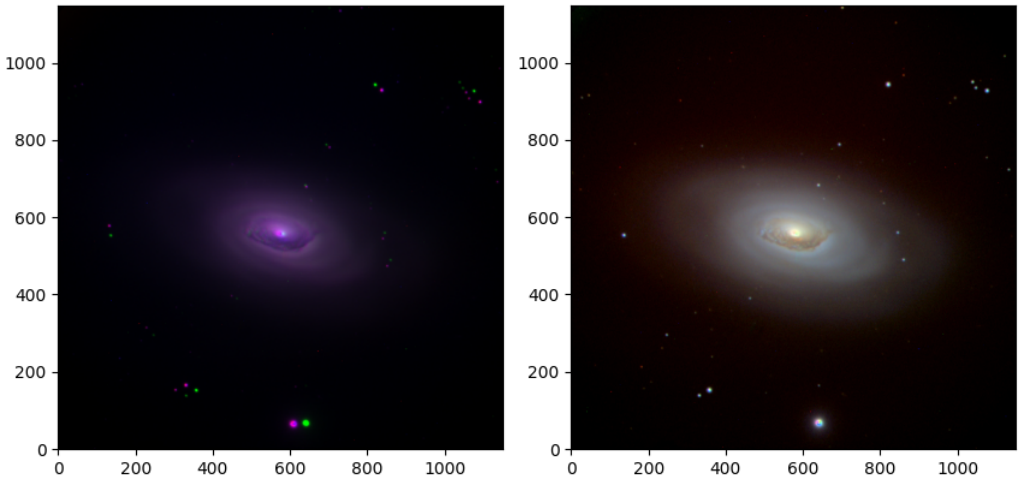


Figure 17: After Stacking

3.2 Spectroscopy

For the spectroscopic analysis of the Galaxy, we focused on studying three main regimes of the galaxy: the bulb, the disk and the full galactic spectrum. In choosing the sky strips of the images, the selection criteria was done in a ’trial-and-error’ way. Different sky strips were tried until we found one for which the resulting spectra were as aligned as possible, since the interpolation, while correcting for misalignments, is not perfect.

3.2.1 Full galactic spectrum

To properly capture the whole galaxy’s spectrum, we take a strip between pixels 500 and 900, and the sky between pixels 270 and 320 as shown in the top panel of figure 18. The middle panel shows the galactic spectrum and sky spectrum (scaled due to the different pixel coverage) and, lastly, the bottom panel shows the spectrum with the sky subtracted from it. It is this spectrum that we multiply by the detector’s response function in order to obtain the true spectrum, shown in the top panel of figure 19.

The first thing we notice in the spectrum is the fact that the galaxy is brighter in red than in blue. This is probably due to the galaxy containing old stellar populations which shine more strongly in the red. We note that in the subsequent analysis the light will be dominated by the bulb, as it is the brightest part, while receiving a contribution from the disk. In the middle and lower panels of figure 19 we zoom into this spectrum and try to find different lines. Firstly, we note in the second panel that we can recognise some important lines, as are [OII] lines at around 3800 Å (their true value is 3726 and 3728.8 Å, however instrumental errors and other

effects most probably have affected the wavelengths; this will happen with more obvious lines as we will see). We also find [SII] lines and even an $[H\beta]$ line. All these are expected since we are including in our spectrum the whole galaxy, with a lot of star forming regions. In the third panel we observe some of the (more clear) lines which we were searching for: the $[H\alpha]$ line (6563 Å) and the two [NII] (6548.1, 6583.3 Å) lines (we note the resolution only allowed for resolving the hydrogen line and one of the nitrogen ones). Again, the wavelengths are shifted due to currently unknown effects, but there is no doubt that these lines are the ones mentioned. Even further, we find the [SII] (6716.4, 6730.8 Å) lines, but these could not be resolved so appear as a single peak in the spectrum. The bottom panel shows the longer wavelength end and, as we can see, the spectrum is very noisy. We recognised the [SIII] (9530.6 Å) line, however it is difficult to know whether this is truly a line or simply a noise peak in the spectrum, as it is not wide.

3.2.2 Bulb spectrum

We now look at the bulb's spectrum. To do so, we choose a strip between pixels 692 and 729 for the spectrum, and 300 to 400 for the sky. In figure 20 we show the strip selection, the raw and sky spectra, and the subtracted sky spectrum. We then change it to real flux units using the response curve and plot this in the top panel of figure 21. We note, again, that the bulb shines more strongly in the red. This is again expected due to the fact that the bulb contains older stellar populations and dominates the spectrum's luminosity. In the middle panel we are able to locate the two [SII] lines (4068.7, 4076.4 Å) resolved separately, and the $[H\beta]$ line (4861 Å). Lastly, in the bottom panel we find the strong $[H\alpha]$ line, the (unresolved) [NII] lines and the [SII] unresolved lines. The longer wavelength range was too noisy to be investigated.

3.2.3 Galactic Disk

Lastly, we investigate the spectrum of the galactic disk, removing the bulb's spectrum. We choose for the spectrum a strip of pixels between 729 and 900, and a sky strip between pixels 250 and 300, as shown in the top panel of figure 22. In general the spectrum is much weaker. We also show, similarly as before, in the middle and bottom panels the raw and sky spectrum, and the subtracted sky spectrum. After calibrating we obtain the spectrum from the top panel of figure 23. This again shines in the red, indicating old stellar populations. In the middle and bottom panels we were able to find [OII], $[H\alpha]$ and [NII] lines, however these lines were much weaker, especially the OII case. The longer wavelength range could not be resolved.

Lastly, we plotted in figure 24 the spectra of the left and right ends of the disk to search for a redshift difference due to the rotation, but no evident redshift appears in the plot. Only a slight intensity (vertical) displacement.

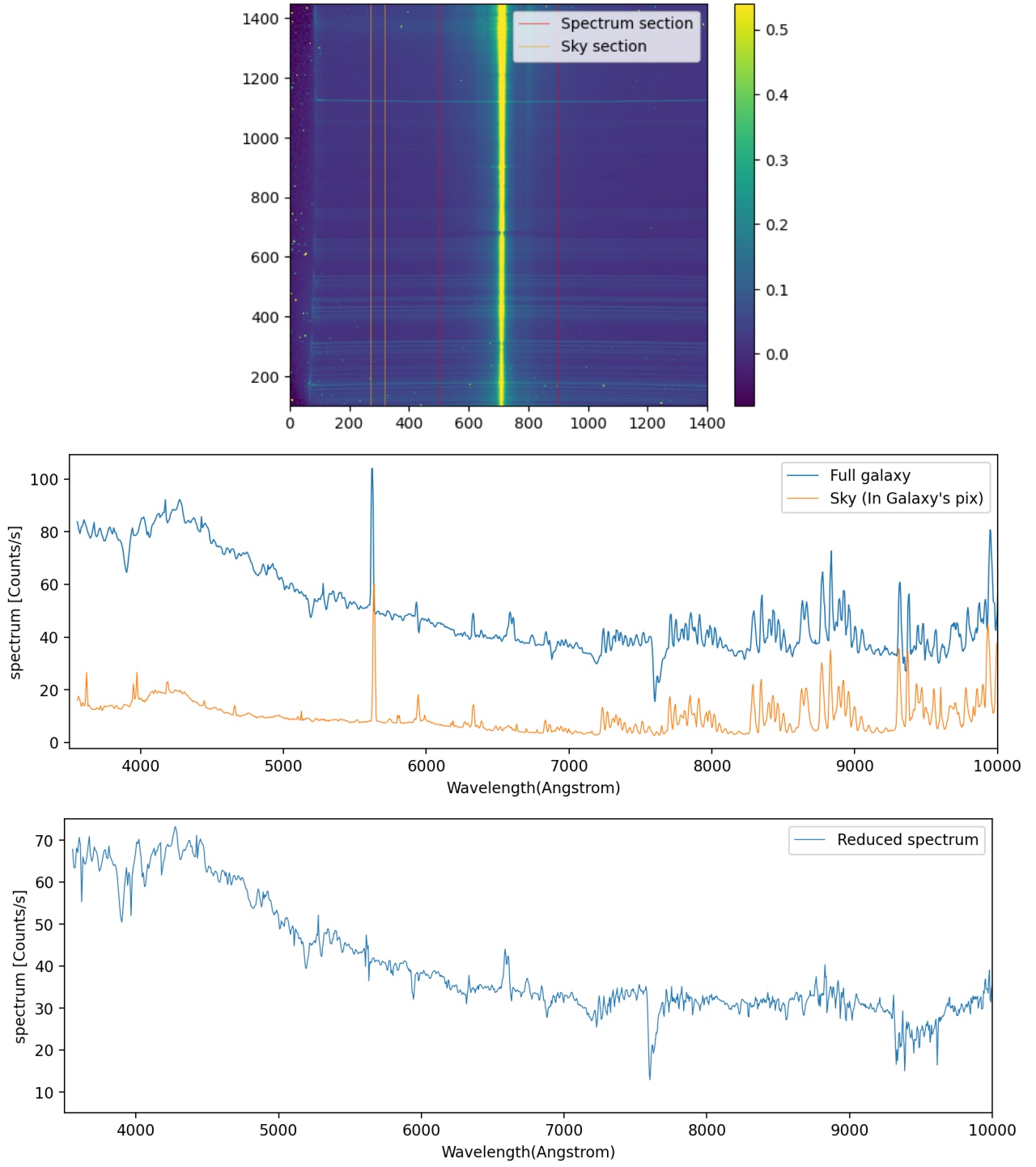


Figure 18: Top panel shows the selected strips for the galactic (limited by the red lines) and sky (limited by the orange lines) spectra. Middle panel shows the sky and galactic spectra, and bottom panel shows the spectrum having subtracted the sky.

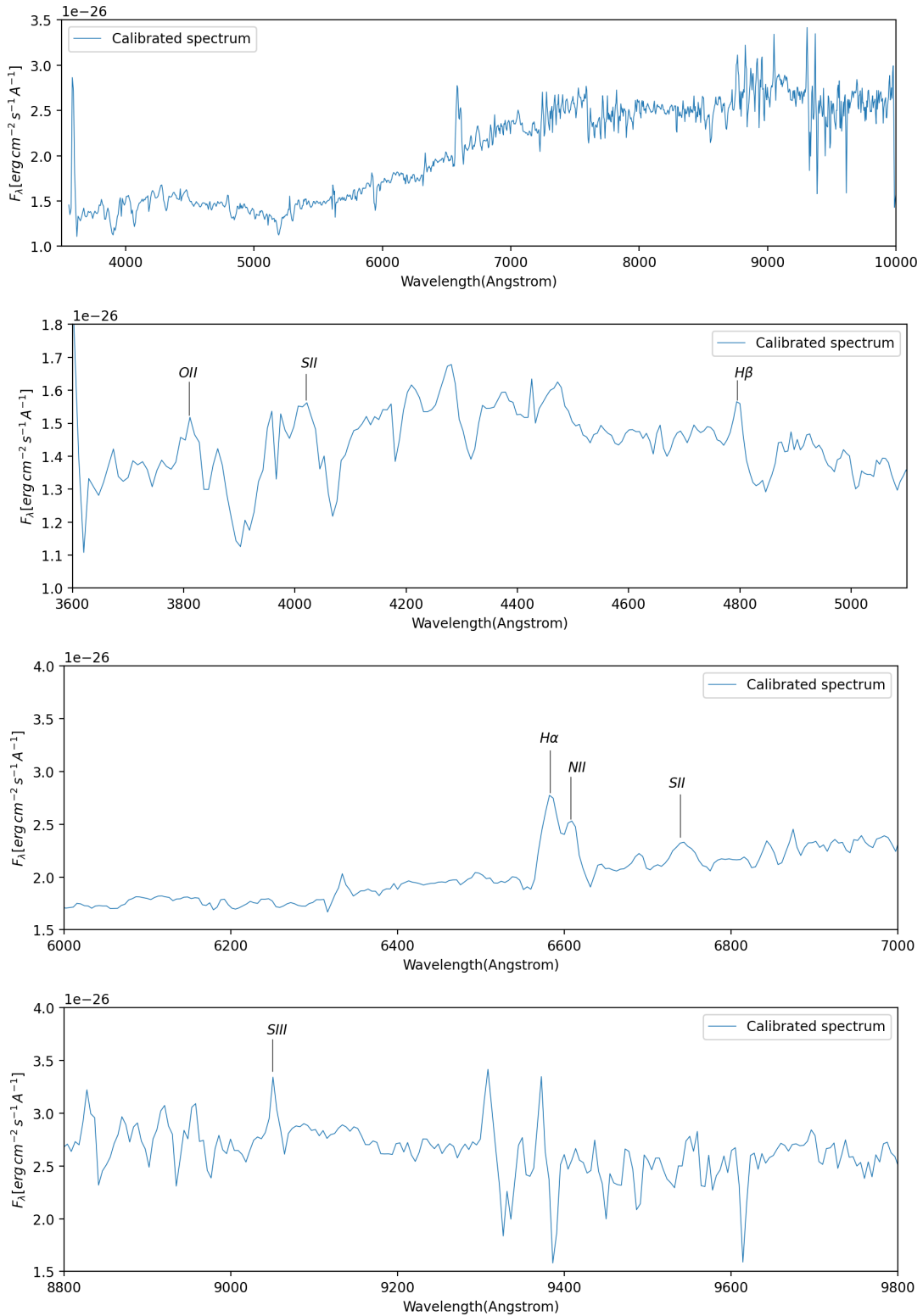


Figure 19: Calibrated full galaxy spectrum (top panel), and zoom into different parts of the spectrum (bottom three panels), with recognised lines.

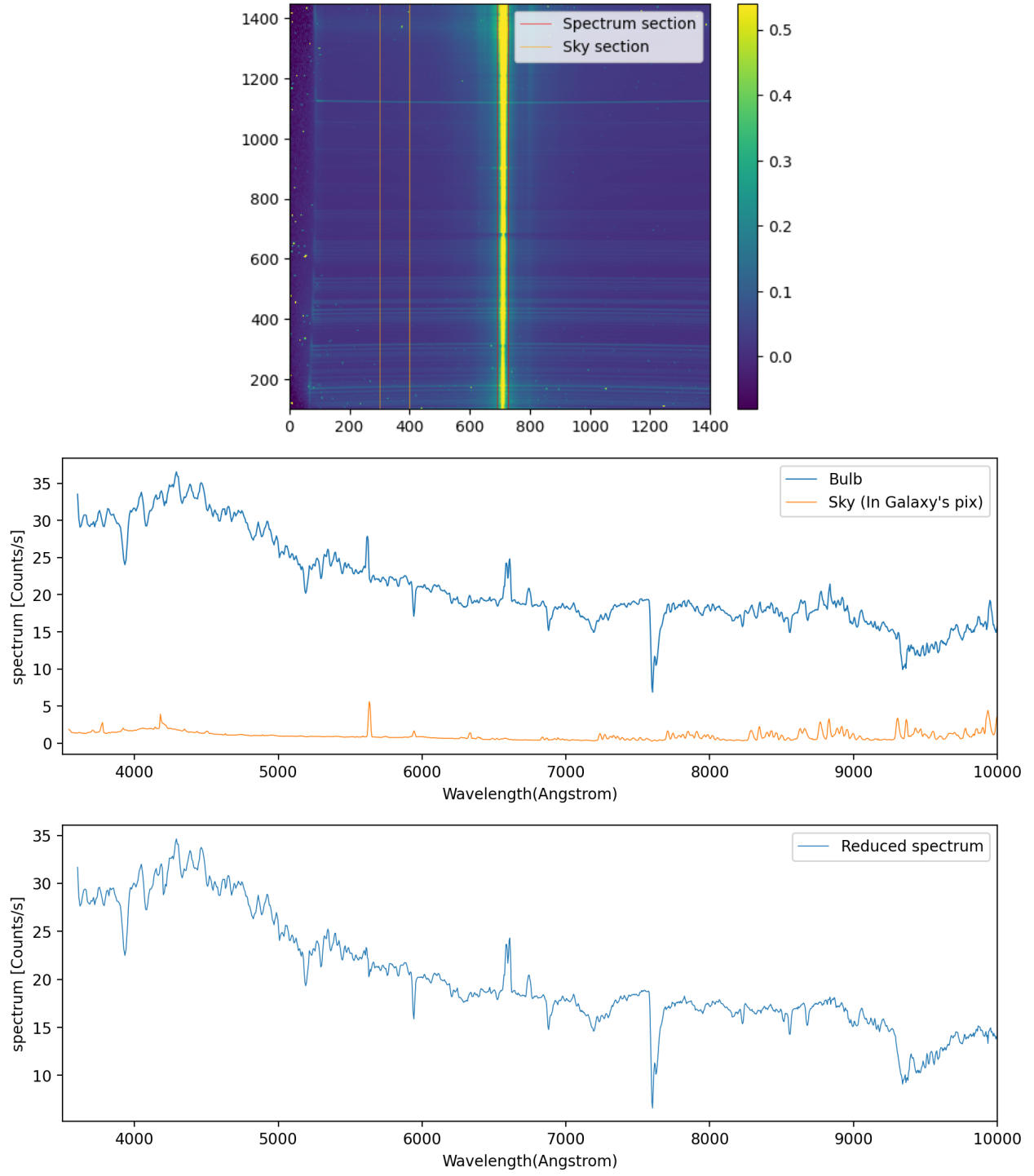


Figure 20: Top panel shows the selected strips for the bulb (limited by the red lines) and sky (limited by the orange lines) spectra. Middle panel shows the sky and bulb spectra, and bottom panel shows the spectrum having subtracted the sky.

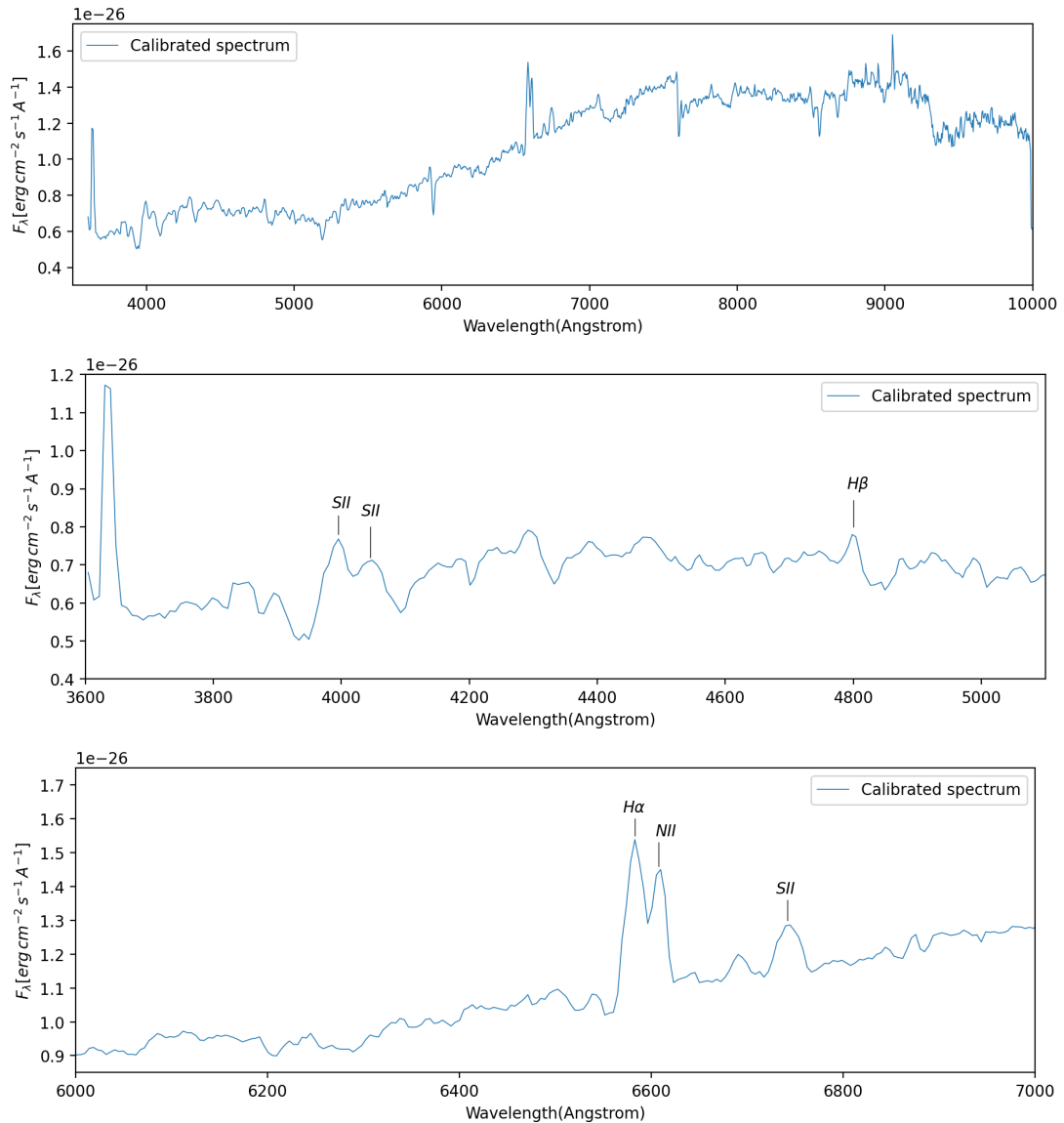


Figure 21: Calibrated bulb spectrum (top panel), and zoom into different parts of the spectrum (bottom three panels), with recognised lines.

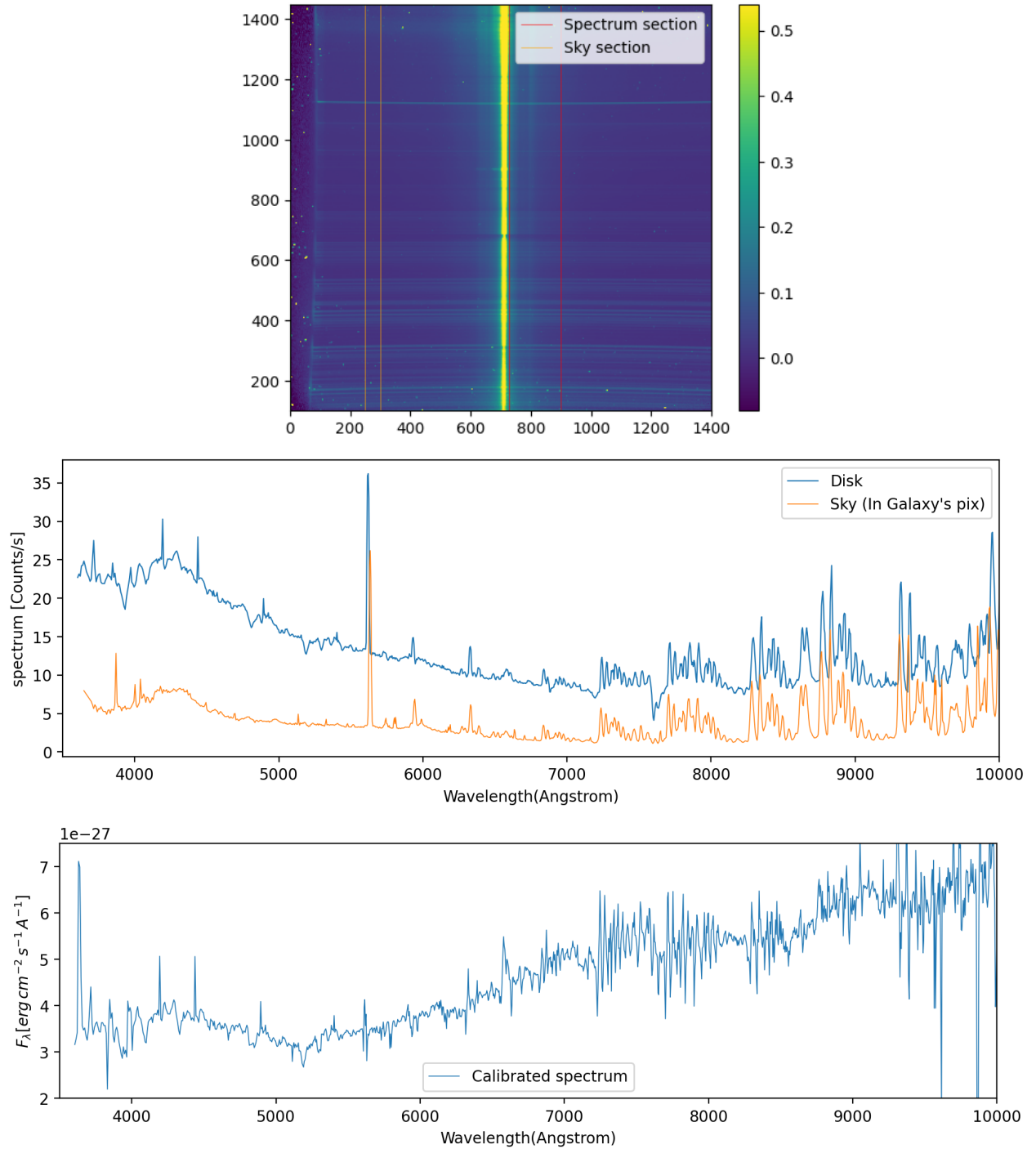


Figure 22: Top panel shows the selected strips for the disk (limited by the red lines) and sky (limited by the orange lines) spectra. Middle panel shows the sky and disk spectra, and bottom panel shows the spectrum having subtracted the sky.

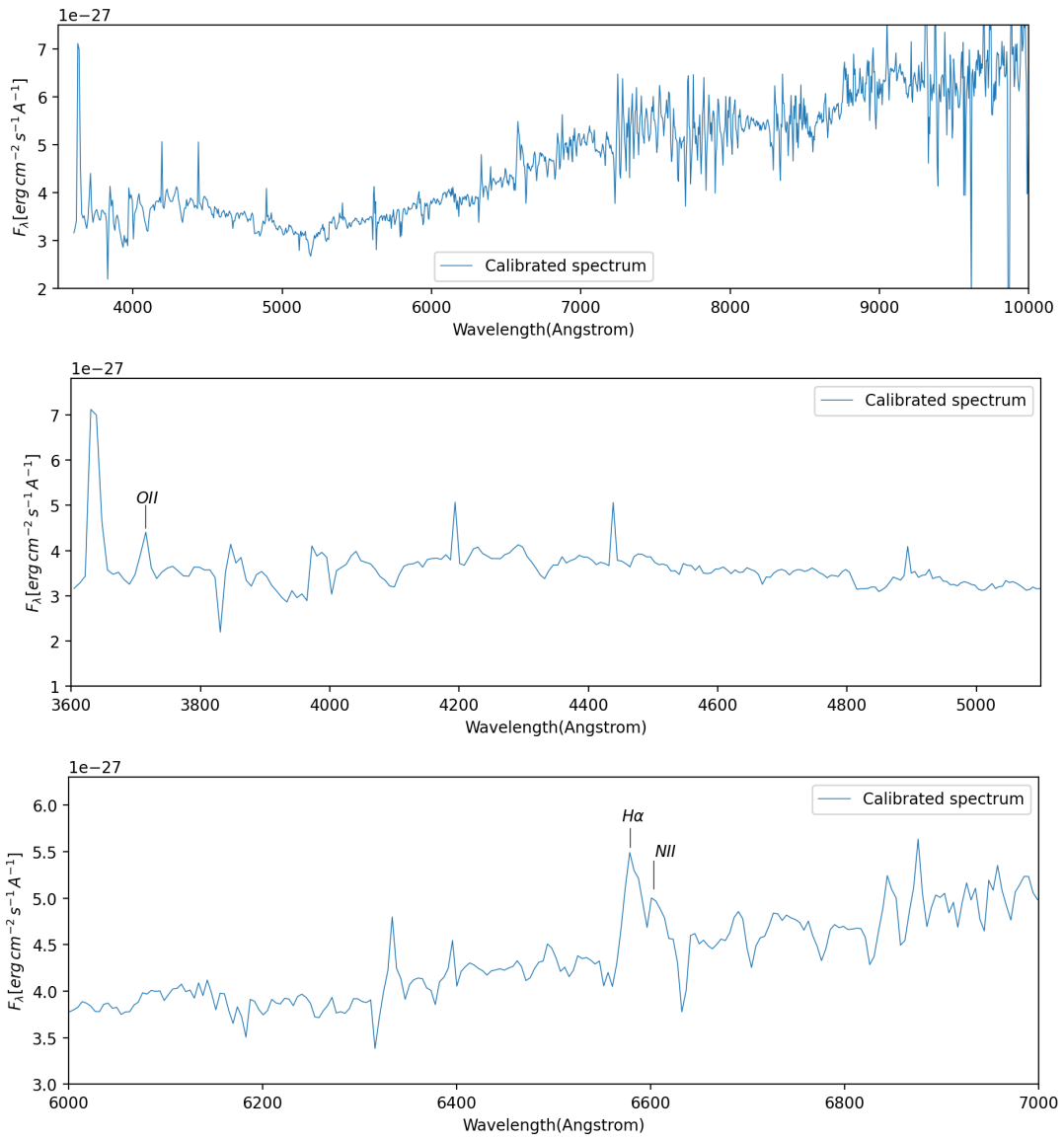


Figure 23: Calibrated disk (right edge) spectrum (top panel), and zoom into different parts of the spectrum (bottom three panels), with recognised lines.

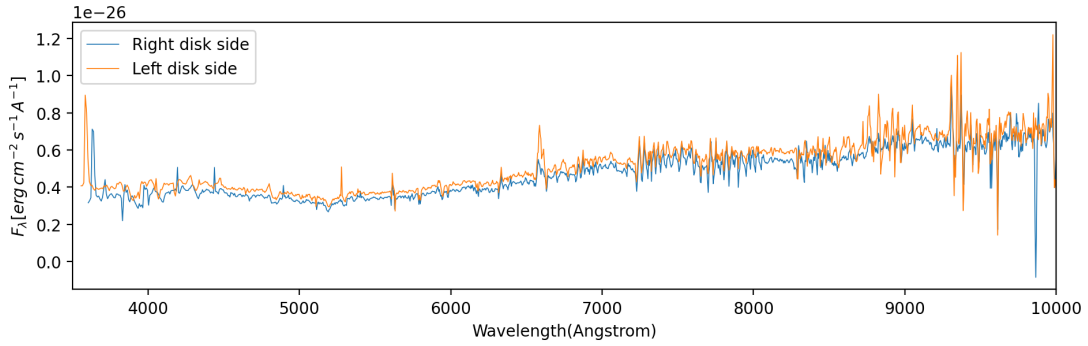


Figure 24: Left and right ends of the disk spectra overlapped.

4 Bibliography

- [1] G. Rauw, T. Morel, and M. Palate. The nature of the high Galactic latitude O-star HD 93521: new results from X-ray and optical spectroscopy. Oct. 2012. doi: 10.1051/0004-6361/201219865
- [2] A repository of Filter information for the VO (CAB INTA-CSIC).
<http://svo2.cab.inta-csic.es>
- [3] The Data Release Seven of LAMOST Low-Resolution Spectroscopic Survey (LRS).
<https://dr7.lamost.org>
- [4] An application to visualise astronomical data.
<https://sky.esa.int>